MODELLING DUST GRAIN IONISATION AND DYNAMICS IN FLAT LEPTON BEAMS USING A SLICED APPROACH

P. Ziegler[1,2*], A. Lechner[2], R. Schmidt[3], C. Wiesner[2], D. Wollmann[2], H. Podlech[1,4]
[1]Goethe-Universität Frankfurt am Main, Germany, [2]CERN, Geneva, Switzerland
[3]Technische Universität Darmstadt, Darmstadt, Germany
[4]Helmholtz Research Academy Hesse for FAIR (HFHF),
GSI Helmholtzzentrum für Schwerionenforschung, Campus Frankfurt

Abstract

Interactions of dust grains with the particle beams can degrade the performance of modern high-intensity accelerators. Existing models developed for the LHC assume grains smaller than the beam size and therefore a spatially uniform primary-particle flux through the grain. This approximation breaks down in flat lepton beams, where the vertical beam size can be smaller than the dust grain.

To describe this regime, a model is introduced for the ionisation and dynamics of dust grains interacting with electron, positron, and proton beams. The grain is discretised into slices, allowing position-dependent ionisation to be treated spatially. The equation of motion is solved with a time-dependent charge using an ionisation model adapted to flat-beam geometries. Application to representative FCC-ee and SuperKEKB parameters provides first quantitative estimates of the penetration depth of charged dust grains.

INTRODUCTION

Dust grains interacting with the beams in the Large Hadron Collider (LHC) typically have diameters of $\sim(1-100)\,\mu\mathrm{m}$ [1]. Even the largest grains are therefore smaller than the typical transverse root mean square (rms) beam size in the LHC arcs of $\sigma \sim (200-300)\,\mu\mathrm{m}$. The simulation code developed for the LHC [2–4] describes the dynamics of dust grains interacting with the beam, including ionisation processes due to secondary electron emission, and approximates the flux of primary particles (pp) over the dust cross-section as constant.

The dynamics shift significantly for lepton machines, such as SuperKEKB [5] and the Future Circular Collider (FCC-ee) [6], where the beams are flat with the vertical size often being smaller than the dust grain diameter. As the flux of pp within the dust grain is no longer homogeneous, the ionisation rate changes locally. Understanding the interaction in this regime is crucial for assessing potential dust-induced limitations.

This paper introduces a model adapted to flat-beam geometries, which discretises the dust grain into slices to describe the stepwise ionisation. This enables a spatially resolved description of the charging process, providing quantitative estimates of dust dynamics for the FCC-ee.

* philipp.ziegler@cern.ch

MODEL

The numerical model builds on the simulation approach of [2–4]. It is assumed that a spherical dust grain with radius R and initial charge Q_0 is located on the beam screen or vacuum chamber surface. The grain is subject to the electrostatic field E of the monochromatic particle beam, described by the Bassetti–Erskine formalism [7], as well as gravity. Adhesive and image forces are neglected. Depending on Q_0 and the initial position and velocity, the electrostatic force accelerates the grain towards the beam centre.

As the grain approaches the beam, halo particles penetrate it and transfer energy to bound electrons through positron–electron (Bhabha, e^+e^-), electron–electron (Møller, e^-e^-), or proton–electron (p^+e^-) scattering. If enough energy is transferred, secondary electrons escape the dust, leading to positive charging. The ionisation rate $\dot{Q}$ therefore depends on the flux and energy of the incident beam particles.

For FCC-ee, the beams are flat, with an average vertical beam size $\sigma_y = 10\,\mu\mathrm{m}$ and horizontal beam size $\sigma_x = 600\,\mu\mathrm{m}$ [6]. A grain with radius $R = 25\,\mu\mathrm{m}$ is therefore much larger than σ_y, so both the particle flux through the grain and the charging become strongly position dependent.

To account for this, the dust grain is sliced along the y-axis into N layers of thickness $\Delta y = 2R/N$, as shown in Fig. 1.

It is assumed that the dust grain starts with initial charge Q_0 from the initial position $\vec{r}_0 = (0, \pm h_{bs}/2)$ from either the bottom or top of the beam screen or vacuum chamber with height h_{bs}. Interactions with the surrounding surface are neglected. The charging of each slice $\dot{Q}_n$ during the passage through the beam is determined by the flux of pp $\Phi_{pp,n}$ through the slice n over the longitudinal interaction

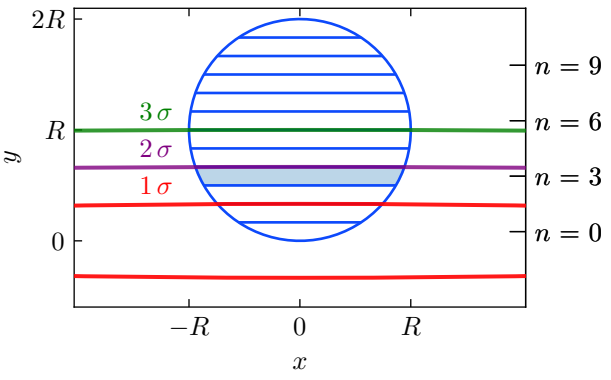

Figure 1: The spherical dust grain is sliced along the vertical axis (y) to account for the varying flux of beam particles.

distance $\mathscr{S}_n$. The ionisation of the material depends on the energy of the monochromatic beam particles:

$$\dot{Q} = \sum_n \dot{Q}_n = \sum_n \left[\left(\int_{\mathscr{A}_n} \mathrm{d}A J_{\mathrm{pp}}(x,\, y) \right) \left(\int_{\mathscr{S}_n} \mathrm{d}z \right) \times \left(\int_{E_{\mathrm{min},n}}^{E_{\mathrm{max}}} \mathrm{d}E\, \rho \frac{\mathrm{d}\sigma_{\mathrm{pp}\to \mathrm{e}^-}(E_{\mathrm{min},n},\, E)}{\mathrm{d}E} \right) \right], \tag{1}$$

with constant density ρ of the dust grain material, current density of pp J_{pp} over the beam-dust cross-section $\mathscr{A}_n$ and differential cross-section $\mathrm{d}\sigma_{\mathrm{pp}\to \mathrm{e}^-}/\mathrm{d}E$.

This leads to the equation of motion:

$$\ddot{y} = \frac{\sum_n Q_{\mathrm{Dust},n}(t)}{m} E_y(y) - g, \tag{2}$$

where m is the dust grain mass, $Q_{\mathrm{Dust},n}(t)$ is the time-dependent charge of slice n, g is the gravitational acceleration, and $E_y(y)$ is the vertical electric field component generated by the beam.

Beam particles propagate along the z-axis while the dust-cross-section lies within the xy-plane. The beam is assumed to be centred around (0, 0). Averaging all paths parallel to the z-axis through the slice yields the geometric mean path:

$$\langle \mathscr{S}_n \rangle = \frac{\pi}{2} \sqrt{R^2 - \left(R - \left(n + \frac{1}{2} \right) \Delta y \right)^2}. \tag{3}$$

Minimum Energy of Kicked Electrons

After scattering, electrons require a minimum kinetic energy T_{min} to reach the surface. The path length of an electron in the material is linked to its kinetic energy T via:

$$r(T) = \frac{\mathrm{A}T}{\rho} \left(1 - \frac{\mathrm{B}}{1 + \mathrm{C}T} \right), \tag{4}$$

with empirically derived constants $\mathrm{A} = 5.37 \times 10^{-6}\,\mathrm{kg/(m^2\,eV)}$, $\mathrm{B} = 0.9815$ and $\mathrm{C} = 3.123 \times 10^{-6}/\mathrm{eV}$ [8].

In [4], FLUKA simulations conclude that the overall ionisation rate agrees with simulation for a mean path length of the electron of $0.3216\,R$. In order to derive the correct path-length-energy equivalent from any slice n, an analytical expression for this finding is required. Minimally scattered electrons move perpendicular to the direction of motion of the incoming primary particle [9] and therefore in the xy-plane.

The mean value of all shortest path lengths from any point inside the sphere to its surface can be calculated as:

$$\langle L_{\mathrm{min}} \rangle = \frac{1}{\frac{4}{3}\pi R^3} \int_{\mathscr{V}} \sqrt{R^2 - z^2} - \sqrt{x^2 + y^2} \mathrm{d}V \approx 0.29\,R. \tag{5}$$

Electrons with T_{min} corresponding to the red line in Fig. 2 reproduce the ionisation rate defined in Eq. (1), in agreement with the simulations reported in [4]. In contrast, using the mean path length in the xy plane underestimates the ionisation rate relative to Garfield [2] and FLUKA [4], whereas the mean shortest path length gives better agreement.

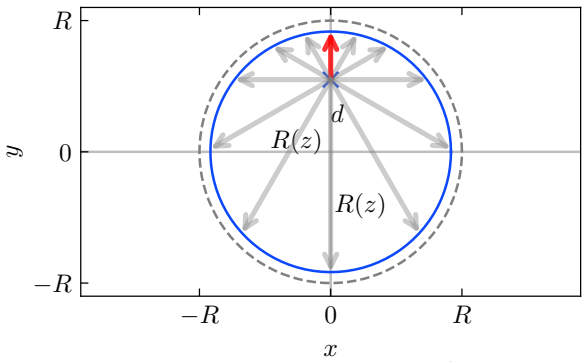

Figure 2: The shortest possible path out of the sphere perpendicular to the motion of the impacting primary particle. d is the transverse offset of the impacting primary particle and $R(z)$ the radius of the cross-section at depth z.

To derive $E_{\mathrm{min},n}$, the mean shortest exit length $\langle L_{\mathrm{min}} \rangle_n$ is evaluated for slice n. In the limit $\Delta y \to 0$, averaging the shortest path in the xy plane over the slice cross section $\mathscr{A}_{y,n}$ yields

$$\langle L_{\mathrm{min}} \rangle_n = \frac{1}{\pi r^2(y_n)} \iint_{\mathscr{A}_{y,n}} \left(\sqrt{R^2 - z^2} - \sqrt{x^2 + y_n^2} \right) \mathrm{d}x\, \mathrm{d}z, \tag{6}$$

with $r(y_n) = \sqrt{R^2 - y_n^2}$. The corresponding minimum energy required for an electron in slice n to reach the surface is then

$$E_{\mathrm{min},n} = r^{-1}(\langle L_{\mathrm{min}} \rangle_n) + \frac{Q}{4\pi\epsilon_0 R}\, \Theta(Q), \tag{7}$$

where the second term accounts for the electrostatic potential barrier of a positively charged grain.

Cross Sections

The maximum energy transferable from one particle to the other is defined as [10]:

$$W_{\mathrm{max}} = \frac{2 m_{\mathrm{e}} \mathrm{c}^2 \beta^2 \gamma^2}{1 + 2\gamma m_{\mathrm{e}}/M + (m_{\mathrm{e}}/M)^2}, \tag{8}$$

where m_{e} is the electron mass, c is the speed of light, β and γ are the relativistic velocity and Lorentz factor of the primary beam particles, and M is the mass of the primary particle ($M = m_{\mathrm{e}}$ for electron or positron beams). For electron-electron scattering, $E_{\mathrm{max}} = W_{\mathrm{max}}/2$, while for positron-electron scattering $E_{\mathrm{max}} = W_{\mathrm{max}}$ [10, 11].

With the relativistic high-energy differential cross-sections defined in [11], and $C = 2\pi \mathrm{N_A} \mathrm{r_e^2} \mathrm{m_e} \mathrm{c}^2 \frac{Z}{A}$, where $\mathrm{N_A}$ is the Avogadro constant, $\mathrm{r_e}$ the classical electron radius, $\mathrm{m_e}$ the electron mass, c the speed of light in vacuum, Z the atomic number of the target material, and A its molar mass, the integrated cross-section for $\mathrm{e^+e^-}$ scattering is:

$$\sigma_{\mathrm{e^+e^-}}(E_{\mathrm{min},n}, E_{\mathrm{max}}) = C \Bigg[\frac{4}{3E_{\mathrm{max}}} + \frac{1}{E_{\mathrm{min},n}} - \frac{3E_{\mathrm{min},n}}{E_{\mathrm{max}}^2} + \frac{E_{\mathrm{min},n}^2}{E_{\mathrm{max}}^3} - \frac{E_{\mathrm{min},n}^3}{3E_{\mathrm{max}}^4} - \frac{2\log\left(E_{\mathrm{max}}/E_{\mathrm{min},n}\right)}{E_{\mathrm{max}}} \Bigg]. \tag{9}$$

and for e^-e^-:

$$\sigma_{e^-e^-}(E_{\min,n}, E_{\max}) = C\left[\frac{E_{\max} - 2E_{\min,n}}{2E_{\max}^2} + \frac{1}{E_{\min,n}} - \frac{1}{E_{\max} - E_{\min,n}}\right]. \quad (10)$$

Despite the difference in maximum transferable energy, the integrated cross-section is almost identical for e^-e^-, e^+e^- and p^+e^- scattering for energies above 1 GeV.

Flux of Primaries in the n-th Slice

With the centre of the dust grain at $(0, y_0)$ and centre of the beam at $(0, 0)$, the slice boundaries are $y_{\min,n} = y_0 - R + n\Delta y$ and $y_{\max,n} = y_{\min,n} + \Delta y$. To account for halo particles, the transverse beam profile is modelled by a double-Gaussian distribution: 80 % of the particles are assumed to follow a Gaussian with width σ_y, while the remaining 20 % are described by a broader Gaussian with width $2\sigma_y$. The number of pp traversing the n-th slice with $R_y = \sqrt{R^2 - y^2}$ is then given by

$$\Phi_{pp,n} = \frac{N_{tot}}{\sqrt{2\pi}} \int_{y_{\min,n}}^{y_{\max,n}} dy \left[\frac{0.8}{\sigma_y} \exp\left(-\frac{y^2}{2\sigma_y^2}\right) \operatorname{erf}\left(\frac{R_y}{\sqrt{2}\sigma_x}\right) + \frac{0.2}{2\sigma_y} \exp\left(-\frac{y^2}{2(2\sigma_y)^2}\right) \operatorname{erf}\left(\frac{R_y}{\sqrt{2}\sigma_x}\right)\right]. \quad (11)$$

Ionisation Yield and Charge Update

Equation (2) needs to be solved stepwise to account for the change of Q. During each integration step, the values of ΔQ_n are calculated. Since the charge relaxation time in conductors [12, p. 130] is approximately 10^9 times shorter than the FCC-ee bunch spacing of 25 ns, all ΔQ_n are accumulated into Q within one integration step.

Beam Losses

From the solved dust trajectory, beam losses defined as number of inelastic collisions integrated over the whole interaction time can be derived for a material with macroscopic cross-section σ_{macro} following [2–4]:

$$\dot{N}(t) = \sum_n \Phi_{pp,n} \sigma_{macro} \langle \mathscr{S}_n \rangle . \quad (12)$$

APPLICATION

As a cross-check, the previous simulation code, Constant Model (CM), from [2–4] is compared with the new model, Sliced Model (SM), using LHC parameters. For a static dust grain with radius 25 µm centred at $(0, 3\sigma_y)$, the ratio r of SM- to CM-flux is 0.9999 for $\sigma_y = 200$ µm, showing that both flux descriptions agree for large beam sizes. For a full trajectory starting at the top centre of the LHC beam screen with initial charge $Q_0 = -1.17$ pC, the CM predicts a slightly larger beam penetration by approximately $0.1\sigma_y$, as shown in Fig. 3. This difference is mainly caused by the updated treatment of the minimum escape energy of knock-on electrons, which yields a charging rate approximately 15 % higher than that of the CM.

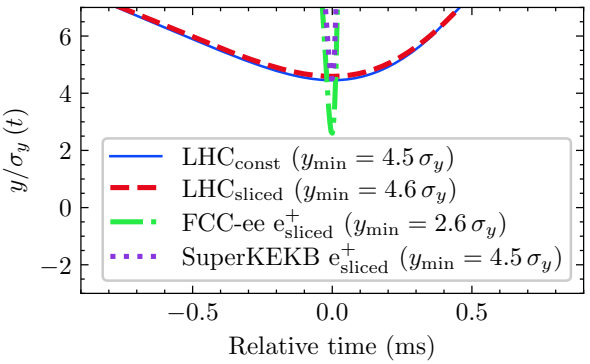

Figure 3: Comparison of trajectories in different particle accelerators for dust with equal initial parameters.

For $\sigma_y = 10$ µm, the ratio of SM- to CM-flux increases to $r = 4.5$. The CM then overestimates the beam losses and penetration depth by 1.4 and 1 σ_y, respectively, while underestimating the beam-loss rise time by 1.7.

Figure 3 shows simulated trajectories in different accelerators for spherical copper dust grains with radius 25 µm, initial charge −3 pC, and initial position at the top of the corresponding beam screen or vacuum chamber. The grains are assumed to be attracted toward the beam with zero initial velocity, using nominal beam parameters with sizes and intensities from SuperKEKB [13], FCC-ee [6], and the LHC [14].

Due to the smaller vertical beam sizes of the lepton beams, dust ionisation processes begin later and more abruptly, resulting in a larger penetration depth and faster ejection of the dust grain compared to LHC parameters.

CONCLUSION

A sliced model for the ionisation and dynamics of dust grains in flat lepton beams was presented. By discretising the grain along the vertical axis, the spatially varying flux of primary particles across the grain volume can be taken into account, which is essential when the beam size is comparable to or smaller than the dust size. The model uses as input the beam parameters, dust radius and material properties, together with the initial grain position, velocity, and charge, and returns the time-dependent grain charge and trajectory.

For large grains in flat beams, the non-uniform primary flux leads to different charging and therefore modified trajectories compared with the non-sliced approximation, whereas for sufficiently small grains both approaches agree well. The model thus provides a framework for quantitatively studying dust motion in lepton machines and for assessing possible dust-induced perturbations of beam operation.

ACKNOWLEDGEMENTS

This work is supported by the Wolfgang Gentner Programme of the German Federal Ministry of Education and Research (grant no. 13E18CHA).

REFERENCES

[1] A. T. Pérez Fontenla, "Analysis and possible sources of dust particles extracted from the LHC", Slides, Workshop on Dust Charging and Beam-Dust Interaction in Particle Accelerators, Geneva, Switzerland, Jun. 2023, https://indico.cern.ch/event/1272104/contributions/5349341/attachments/2665563/4618966/Analysis%20and%20possible%20sources%20of%20dust%20particles%20extracted_14.06.23.pdf (visited on 02/18/2026),

[2] B. Auchmann *et al.*, "Proton-beam macro-particle interation: beam dumps and quenches", CERN, Rep. CERN-ACC-NOTE 2020-0041, 2014. https://cds.cern.ch/record/2727938

[3] S. Rowan *et al.*, "Interactions between macroparticles and high-energy proton beams", in *Proc. IPAC'15*, Richmond, VA, USA, May 2015, pp. 2112–2115, 2015. doi:10.18429/JACoW-IPAC2015-TUPTY045

[4] B. Lindstrom *et al.*, "Dynamics of the interaction of dust particles with the LHC beam", *Phys. Rev. Accel. Beams*, vol. 23, no. 12, p. 124501, 2020. doi:10.1103/PhysRevAccelBeams.23.124501

[5] K. Ohmi, H. Fukuma, and S. Terui, "Beam-dust interactions in an e^+e^- collider", *arXiv*, Jan. 2025. doi:10.48550/arXiv.2510.04415

[6] M. Benedikt *et al.*, "Future circular collider feasibility study report: Volume 2", *Eur. Phys. J. Spec. Top.*, vol. 234, no. 19, pp. 5713–6197, 2025. doi:10.17181/CERN.EBAY.7W4X

[7] M. Bassetti and G. A. Erskine, "Closed expression for the electrical field of a two-dimensional Gaussian charge", CERN, Geneva, Rep., 1980. https://cds.cern.ch/record/122227

[8] E. J. Kobetich and R. Katz, "Energy deposition by electron beams and δ rays", *Physical Review*, vol. 170, p. 391, 1968. doi:10.1103/PhysRev.170.391

[9] L. Rolandi, W. Riegler, and W. Blum, *Particle Detection with Drift Chambers*. Springer Berlin, Heidelberg, 2008. doi:10.1007/978-3-540-76684-1

[10] D. E. Groom and S. R. Klein, "Passage of particles through matter", in in *Review of Particle Physics*, ed. by S. Navas *et al.*, vol. 110, revised Aug. 2023, Particle Data Group, 2024, p. 030001, https://pdg.lbl.gov/2024/reviews/rpp2024-rev-passage-particles-matter.pdf,

[11] B. B. Rossi, *High-Energy Particles*. New York, NY: Prentice-Hall, 1952. https://cds.cern.ch/record/99081

[12] J. Herbert P. Neff, *Introductory Electromagnetics*. New York, NY, USA: John Wiley & Sons, 1991.

[13] K. Ohmi, H. Fukuma, and S. Terui, "Beam-dust interactions in an e^+e^- collider", *Phys. Rev. Accel. Beams*, vol. 29, no. 2, p. 021002, Feb. 2026. doi:10.1103/dwmr-qldc

[14] O. S. Brüning *et al.*, *LHC Design Report*. Geneva: CERN, 2004. doi:10.5170/CERN-2004-003-V-1